Micromechanical simulations of microstructure-sensitive Stage I fatigue crack growth

Véronique Doquet

Micromechanical simulations of microstructure-sensitive Stage I fatigue crack growth

V. DOQUET

Laboratoire de M´ecanique des Solides, UMR-CNRS 7649, Ecole Polytechnique, 91128 Palaiseau cedex, France

ABSTRACT Simulations of dislocation dynamics at the tip of a Stage I crack are performed, taking into account the influence of the normal stress on the friction of the crack flanks and on the condition for dislocation emission at the crack tip. The interactions of the emitted dislocations with microstructural obstacles are analysed. The repeated decelerations and sometimes arrests that characterize Stage I crack growth are properly described by the model, and the differences in Stage I kinetics observed in reversed torsion and push–pull are analysed in terms of crack tip–grain boundary interactions.

Keywords Stage I, multiaxial fatigue, short cracks, grain boundaries, dislocations.

INTRODUCTION

In the first stage of their development, fatigue cracks are driven by cyclic shear, but their growth rate is influenced by the normal stress: it is increased by an opening stress and reduced by a compressive one. In a previous paper,[1] simulations of dislocation dynamics at the tip of a crystallographic mode II crack, ignoring at first the influence of microstructural obstacles, have been presented. The crack growth rates were deduced from the dislocation flux at the crack tip. The normal stress was assumed to affect the growth kinetics through its influence on friction of the crack flanks and on the condition for dislocation emission at the crack tip. Preliminary results were qualitatively consistent with experimental data: a threshold stress intensity factor below which no propagation occurs for lack of cyclic plasticity at the crack tip was found, and for unconstrained slip, the growth of crystallographic mode II cracks was predicted to be slower in torsional fatigue than in push–pull for equivalent stress ranges.

In reality, due to interactions of the emitted dislocations with microstructural obstacles, Stage I crack growth is characterized by repeated decelerations and sometimes arrest that have to be properly modelled if the fatigue life and fatigue limit of structures containing short cracks is to be predicted. Models based on the continuously distributed dislocation theory were proposed by Tanaka *et al.*[2] and Navarro and De Los Rios.[3] These models have some success in describing the irregularities in Stage I kinetics. However, they do not take into account any influence of the normal stress on crack growth, which appears to be a major shortcoming for the analysis of multiaxial fatigue, as, e.g. nothing discriminates push–pull and reversed torsion as concerns Stage I kinetics. This is why the simulations of discrete dislocations emission and glide ahead of a crystallographic mode II crack mentioned above were extended, so as to incorporate the interactions of the dislocations with microstructural obstacles. In the present paper, the results of this approach are compared to those obtained by Tanaka *et al.*[2] or Navarro and De Los Rios.[3]

A BRIEF DESCRIPTION OF THE MODEL FOR UNCONSTRAINED SLIP

The principle of the simulations is only briefly recalled here. More details can be found in Ref. 1. Stage I fatigue cracks grow along localized slip-bands and can be submitted to mode I + II + III loading, but plasticity, i.e. dislocation nucleation and glide, is related only to the shear components and is restricted to the slip band colinear to the crack, otherwise (i.e. if non-coplanar slip is activated) there is a transition towards Stage II propagation.

In the present simulations, only mixed mode I + II loading has been considered for the sake of simplicity. This means that the dislocations that are emitted and glide along the coplanar slip plane have a pure edge character. This was also the case in the recent work by Wilkinson *et al.*,[4] who envisaged an influence of mode I on Stage I crack growth (blunting would enhance slip

irreversibility), but did not explicitly integrate it into their simulations, while Pippan[5] and Caracostas *et al.*[6] consider mode III, and thus screw dislocations, but underline the similitude with mode II.

The possibility of cross-slip is not envisaged here. This means that the present simulations are pertinent essentially for low stacking-fault-energy FCC alloys (or medium SFE alloys at low temperature) as well as for short-range ordered alloys. The possible splitting of dislocations into partials is, however, not represented.

Figure 1 shows the algorithm of the calculations. The cyclic loading path is followed by incremental time steps, Δt, small enough for the velocity of each dislocation to be considered constant over Δt. Two successive cycles only need to be simulated, because the second cycle is representative of the steady-state. The nominal stress intensity factors for a Stage I crack of length $2a$ lying along the critical plane (i.e. the plane where the shear stress range is maximum) are calculated at each time-step as:

$$K_{\mathrm{I}} = \sigma_{\mathrm{ncp}} \cdot \sqrt{\pi a} \quad \text{when } \sigma_{\mathrm{ncp}} \geqslant 0 \qquad K_{\mathrm{II}}^{\mathrm{nom}} = \tau_{\mathrm{cp}} \cdot \sqrt{\pi a} \tag{1}$$

where σ_{ncp} and τ_{cp} are the current values of the normal stress and shear stress on the critical plane. Because real Stage I cracks are not straight, allowance has to be made for asperity-induced friction that tends to reduce the crack driving force, and is either enhanced or reduced by a compressive (respectively tensile) normal stress.

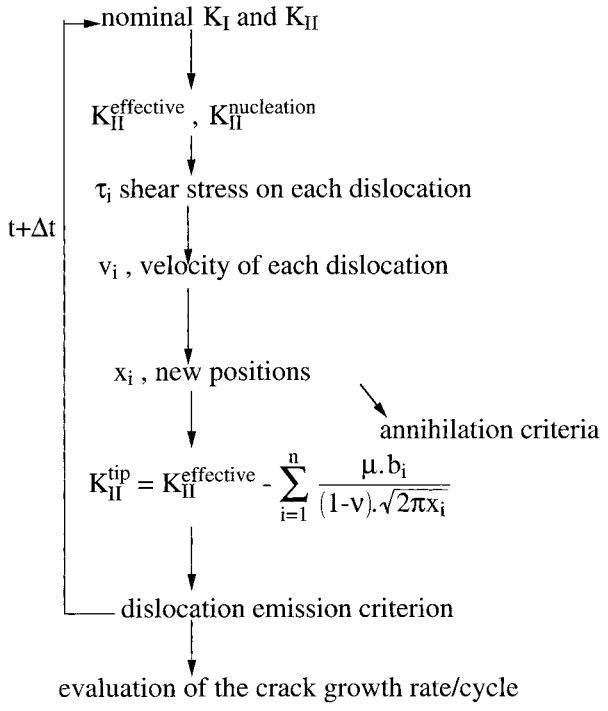

Fig. 1 Algorithm of the simulations.

Experimental information concerning crack flanks frictional interactions for long cracks loaded in mode II, in the presence of a static normal stress, has been obtained through combined tension and torsion tests performed inside a scanning electron microscope on precracked tubular specimens of maraging steel.[1] In the present study, an attempt is made to reproduce qualitatively these experimental data using empirical equations. The effective mode II stress intensity factor is thus calculated, assuming that a uniform, normal stress-dependent friction stress, c, exists along the crack flanks:

$$K_{\mathrm{II}}^{\mathrm{eff}} = K_{\mathrm{II}}^{\mathrm{nom}} \pm c\sqrt{\pi a} \tag{2}$$

with

$$\begin{aligned} c &= c_0 \cdot \exp(-k_+ \cdot \sigma_{\mathrm{ncp}}) \quad \text{if } \sigma_{\mathrm{ncp}} \geqslant 0 \\ c &= c_0 \cdot \exp(-k_- \cdot \sigma_{\mathrm{ncp}}) \quad \text{if } \sigma_{\mathrm{ncp}} \leqslant 0 \end{aligned} \tag{3}$$

c_0 is a constant which characterizes the friction stress in the absence of any normal stress and is thus related to the tortuosity of the crack path. k_+ and k_- are two constants, the latter connected with the friction coefficient of the material. The simulations described below have been performed with values of c_0 between 5 and 20 MPa, $k_+ = 0.057$, $k_- = 0.014$ (this means that c is divided by 100 for $\sigma_{\mathrm{n}} = 80$ MPa, but is multiplied only by three for $\sigma_{\mathrm{n}} = -80$ MPa, consistent with experimental data reported in Ref. 1).

The critical mode II stress intensity factor for the emission of a coplanar edge dislocation from the crack tip, which depends on the mode mixity parameter $\Psi = \arctan(K_{\mathrm{II}}/K_{\mathrm{I}})$, is then calculated, using the expression given by Sun *et al.*:[7]

$$K_{\mathrm{II}}^{\mathrm{nucl}} = \sqrt{\frac{2\mu}{(1-\nu)}\left[\gamma_{\mathrm{us}}^{\mathrm{r}} - \alpha \cdot (\gamma_{\mathrm{us}}^{\mathrm{u}} - \gamma_{\mathrm{us}}^{\mathrm{r}})\left(\frac{\pi}{2} - \Psi\right)\right]} \tag{4}$$

where α, $\gamma_{\mathrm{us}}^{\mathrm{u}}$ and $\gamma_{\mathrm{us}}^{\mathrm{r}}$ are material parameters estimated by atomic models (density functional theory or embedded atom method) and tabulated in Ref. 7 for a few materials, among which are iron, nickel and aluminium. Because $\gamma_{\mathrm{us}}^{\mathrm{u}} > \gamma_{\mathrm{us}}^{\mathrm{r}}$, Eq. (4) predicts a lower threshold stress intensity factor for dislocation nucleation when Ψ decreases, i.e. when an opening stress is present. Figure 2 illustrates this effect for the values of α, $\gamma_{\mathrm{us}}^{\mathrm{u}}$ and $\gamma_{\mathrm{us}}^{\mathrm{r}}$ given in Ref. 7 for nickel and used in the simulations.

The shear stress on each dislocation in the plastic zone is then evaluated as:

$$\tau_i = \frac{K_{\mathrm{II}}^{\mathrm{eff}}}{\sqrt{2\pi x_i}} - \frac{\mu b_i}{4\pi(1-\nu)x_i} - \sum_{j \neq i} \frac{\mu b_j}{2\pi(1-\nu)} \sqrt{\frac{x_j}{x_i}} \cdot \frac{1}{x_j - x_i} + \tau_{\mathrm{cp}} \tag{5}$$

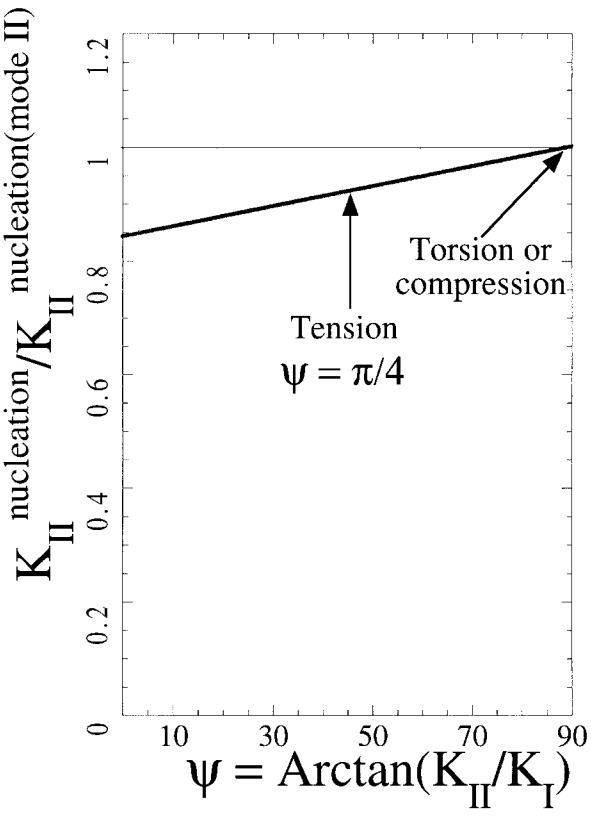

Fig. 2 Evolution of the dislocation nucleation threshold with mode mixity at the crack tip for nickel, according to Sun *et al.*[7].

in which the first three terms represent, respectively, the crack tip stress, image stress and stress of other dislocations. The last term, which had been omitted in Ref. 1, is the far-field term, negligible for dislocations located very close to the crack tip, but more important for leading dislocations, when the size of the plastic zone is a relatively large fraction of the crack size, as will be the case for the short cracks considered below. In the following, however, the size of the plastic zone will never exceed $0.2a$, so that Eq. (5) may be considered a reasonable approximation. In the author's view, anyhow, the crudest approximation is perhaps not the use of an elastic stress field (somewhat corrected for plasticity through dislocations contributions) but rather the direct use of the external loading for the calculation of τ_{cp} and K_{II}^{nom}, without any account for internal stresses as yet. This might be a way for future improvement of the model.

The velocity of each dislocation is then calculated as:

$$v_1 = v_0 \cdot \mathrm{sign}(b_i) \cdot \mathrm{sign}(\tau_i) \cdot \langle |\tau_i| - \tau_f \rangle^m \quad \text{where } \langle x \rangle \text{ is zero if } x \leqslant 0 \text{ and } x \text{ otherwise} \tag{6}$$

τ_f is the resistance to dislocation glide when slip is not constrained by a grain boundary, v_0 and m are two constants. For the simulations described below, τ_f varied between 20 and 90 MPa. Typical values of v_0 and m for FCC metals (13 ms^{-1} and 0.88, respectively) taken from the velocity measurements made on edge dislocations in pure copper by Jassby and Vreeland[8] were chosen.

The new position of each dislocation is then deduced, and annihilation criteria are checked: if a dislocation comes close enough to the crack tip (less than 1 Å), or if the distance between two dislocations with opposite signs becomes less than 16 nm, they are removed from the simulation.

The real mode II stress intensity factor, with allowance made for crack tip shielding by the dislocation stress field, is then evaluated as:

$$K_{II}^{tip} = K_{II}^{eff} - \sum_{i=1}^{n} \frac{\mu b_i}{(1-\nu)\sqrt{2\pi x_i}} \tag{7}$$

The dislocation emission criterion:

$$K_{II}^{tip} \leqslant -K_{II}^{nucl} \quad \text{or} \quad K_{II}^{tip} \geqslant K_{II}^{nucl} \tag{8}$$

is then checked to decide whether a negative or positive dislocation can be emitted.

This sequence is repeated until the second cycle is completed. Then, the crack growth rate per cycle is deduced from the dislocation flux as follows. The crack is considered to grow by one Burgers vector each time a pair of positive–negative dislocations has been emitted at the crack tip, or when a positive (or negative) dislocation returns to the crack tip. In the latter case, it is assumed that even though the crack tip geometry before the dislocation nucleation is, in principle, recovered when this dislocation comes back, the free surface increment created at nucleation, that has been exposed to environment and gas adsorption in the meantime, cannot be rewelded afterwards. Anyway, both events correspond to some cyclic plastic flow at the crack tip and should thus contribute to its growth.

An example set of data used for the simulations, in addition to the shear modulus and Poisson's ratio (70 000 MPa and 0.3, respectively), is given in Table 1.

Figure 3 (published in Ref. 1 with a misprint on the abcissa scale) shows the mode II crack growth rates calculated, for unconstrained slip, in push–pull and reversed torsion, for Tresca equivalent stress ranges, drawn in a bilogarithmic plot, as a function of the nominal ΔK_{II}, for various values of the crack flanks friction stress, c_0. In reversed torsion, where the effective loading is fully reversed and where no opening stress affects the threshold for dislocation emission, the calculated growth rates follow a very simple equation:

$$\frac{da}{dN} = \frac{(1-\nu)}{4 \cdot \mu \cdot b \cdot \tau_f} \cdot (\Delta K_{II}^{eff^2} - 4 \cdot K_{II}^{nucl^2}) \tag{9}$$

c_0 (MPa)	k_+ (MPa^{-1})	k_- (MPa^{-1})	τ_f (MPa)	v_0 (ms^{-1})	m	γ^r_{us} (Jm^{-2})	γ^u_{us} (Jm^{-2})	α	τ_{GB} (MPa)
5	0.057	0.014	20	13	0.88	0.226	0.26	1.2	300

Table 1 Example set of data used in the simulation

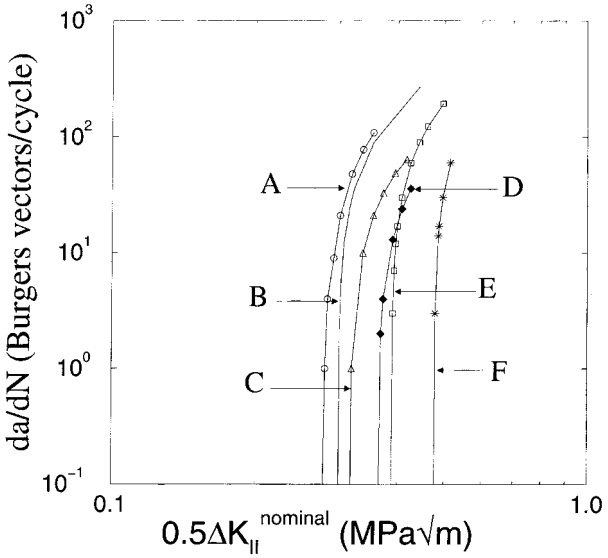

Fig. 3 Comparison of the calculated crack growth rates versus nominal ΔK_{II} curves: (A) push–pull, no friction; (B) reversed torsion, no friction; (C) push–pull, $c_0 = 5$ MPa; (D) push–pull, $c_0 = 10$ MPa; (E) reversed torsion, $c_0 = 5$ MPa; (F) reversed torsion, $c_0 = 10$ MPa (calculations performed with a varying stress range and a constant half crack-length, $a = 100$ μm).

in which K_{II}^{nucl} is the emission threshold in pure shear. The threshold for propagation is thus $2K_{II}^{nucl}$ in that case.

INTERACTIONS WITH MICROSTRUCTURAL OBSTACLES

Influence of an impenetrable obstacle

If there is an impenetrable obstacle ahead of the crack tip, the dislocations emitted by the crack pile up there, and as the crack propagates towards the obstacle, the shielding effect due to the pile up is stronger and stronger [see Eq. (7)]. The increment of K_{II}^{eff} necessary for the emission of a new dislocation is thus higher and higher. As a result, there are fewer and fewer dislocations emitted, even though $\Delta K_{II}^{nominal}$ increases, so that the crack decelerates. When the crack tip is finally so close to the obstacle (e.g. less than the core radius of a dislocation) that there is not enough space for a single dislocation loop to expand from the tip, and anyway the attraction by image forces would make it unstable, the emission criterion of Eq. (8) is not applied any more, as emission becomes physically impossible. The crack is thus considered to stop [if Eq. (8) was still applied, the simulation would diverge, i.e. an endless process of emission–annihilation would occur, which is meaningless]. Strictly speaking, the last position of the tip for which the crack growth rate can be obtained from the simulations is at a distance x_0 from the obstacle, where x_0 is the abscissa of the unstable equilibrium position of a dislocation at a crack tip calculated by Ohr,[9] below which the dislocation is attracted back to the tip

$$\left(x_0 = \frac{(K_{II}\sqrt{1-\nu} - \sqrt{K_{II}^2 \cdot (1-\nu) - 2 \cdot \mu \cdot b \cdot \tau_f})^2}{8 \cdot \pi \cdot (1-\nu) \cdot \tau_f^2}\right)$$

that is a few Angström for the parameters considered here. If the obstacle has not yet been overcome by dislocations when the crack tip is closer than x_0, the crack is considered to stop.

Simulations of stage I growth for two constant stress ranges ($\Delta\tau/2 = 36.95$ MPa and $\Delta\tau/2 = 37.8$ MPa) and thus increasing ΔK_{II}^{nom}, have been performed in reversed torsion ($R = -1$), for a crack of initial half-length $a = 105$ μm approaching an impenetrable obstacle, initially 15 μm away. The friction stress of the material, τ_f, was 30 MPa, and the crack flanks friction stress, c_0, was 20 MPa. Figure 4 shows the evolution of the calculated growth rate. It can be shown that when the maximum applied shear stress is less than τ_f, the crack accelerates, as long as its plastic zone does not reach the obstacle,

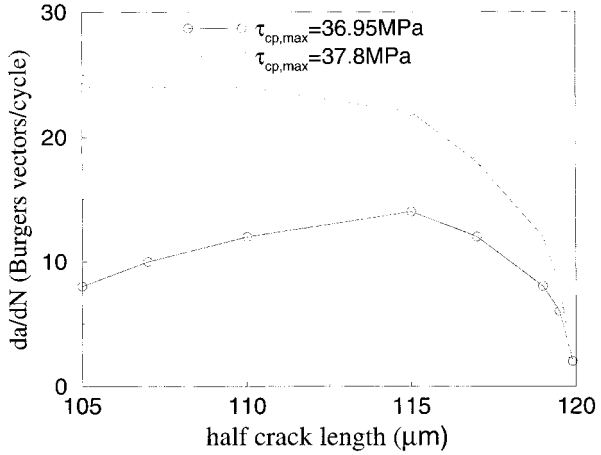

Fig. 4 Evolution of the growth rate for a Stage I crack (initial half-length 105 μm) propagating toward an impenetrable obstacle, initially 15 μm away, in reversed torsion ($c_0 = 20$ MPa, $\tau_f = 30$ MPa).

and then slows down until it stops. But for both cases illustrated in Fig. 4, $\tau_{cp,max} > \tau_f$, so that the crack tip plastic zone hits the obstacle for each crack length considered. But for the smallest stress range considered, the number of dislocations emitted is small, so that down to 5 μm distance from the obstacle, the rise of the shielding term in Eq. (7) is slower than the increase in K_{II}^{eff}, and the crack is able to accelerate in spite of its constrained plastic zone. For the highest stress range considered, on the contrary, the rise of the shielding term approximately compensates that of K_{II}^{eff} at the beginning, and then exceeds it, therefore the constant and then decreasing growth rate.

The influence of an impenetrable obstacle on Stage I kinetics is more complex in push–pull. Figure 5 compares the evolution of the calculated crack growth rates as a function of the distance to the obstacle in push–pull and reversed torsion (here, the obstacle is moved, not the crack tip, and $\Delta K_{II}^{nominal}$ is constant). The maximum applied shear stress, $\tau_{cp,max}$ was 27.2 MPa (which is less than the friction stress chosen here, $\tau_f = 90$ MPa) and c_0 was 10 MPa. Whereas in torsion the growth rate in the presence of an obstacle is always smaller than for unconstrained slip, the obstacle can accelerate the crack growth in push–pull, provided it is not too close. This paradoxical result can be understood in the light of the simulations detailed in Ref. 1. It was shown that in push–pull the return of emitted dislocations to the crack tip, necessary for crack advance, was made difficult by enhanced crack flanks friction in the compressive stage of the cycle: the effective loading was therefore not fully reversed. But if an obstacle limits the size of the plastic zone and keeps the dislocations closer to the crack tip, they are attracted back more easily by the stress field of the crack when it changes sign [see Eq. (5)]. Below a certain distance between the obstacle and crack tip, however, the pile-up shielding effect becomes dominant and the crack growth decreases, as in torsion. Figure 5 also shows that for equal crack lengths and equivalent stress ranges, the range of interaction with the obstacles (which is identical to the size of the plastic zone) is longer in push–pull than in reversed torsion.

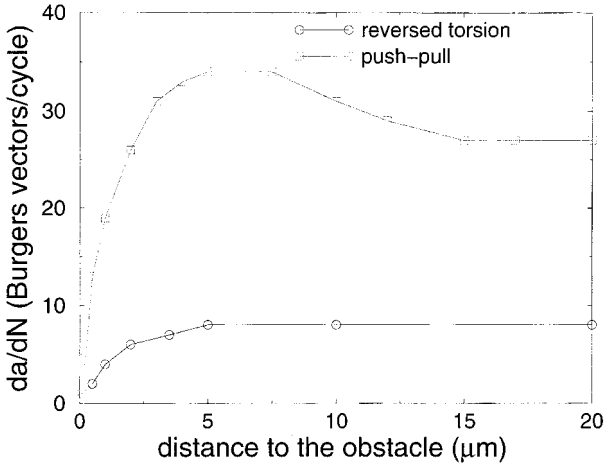

Fig. 5 Influence of an impenetrable obstacle on the Stage I crack growth rates in push–pull and reversed torsion for Tresca equivalent stress ranges ($\tau_{cp,max} = 27.2$ MPa, $\tau_f = 90$ MPa, $c_0 = 10$ MPa).

Influence of grain boundaries

Slip transfer beyond a grain boundary

Grain boundaries (GBs) are generally not impenetrable to dislocations. They can be sinks for incident lattice dislocations as well as effective sources of dislocations. Ohr[9] has made direct observations of crack tip–GB interactions in thin foils loaded in a transmission electron microscope. He reports dislocations annihilating in GBs, while others were emitted at the GBs into the neighbouring grain.

In the present simulations, if the plastic zone at the crack tip reaches a GB, dislocations are assumed to pile up there until the shear stress on the leading dislocation reaches a value allowing it to enter the GB and a new one to glide into the next grain, on a slightly misoriented plane. The geometrically necessary dislocations left at the GB by the incorporation reaction are not taken into account, nor is, explicitly, the tilt of the crack path beyond the GB. But some of it is modelled through the roughness-induced friction stress [Eqs (2) and (3)]. The same criterion is then applied to the following dislocations. This scenario, consistent with Ohr's observations, has an additional advantage: it avoids introducing an ill-defined position for a dislocation source in the next grain, as is done in some short crack models.[3] Similar conditions for grain boundary crossing were introduced by Pippan,[5] and Li and Li[10] in their simulations. The critical shear stress for slip transfer, τ_{GB}, should depend on the crystallographic misorientation of the adjacent grains and on the angle of incidence of the slip plane on the GB plane. Here it is considered as independent of the slip direction (the GBs are also obstacles for dislocations gliding back towards the crack tip at unloading).

Figure 6 shows the positions of the dislocations emitted by a crack tip located 1 μm away from a first GB and 16 μm from a second one, at various points of a load ramp, in torsion. Two cases are considered: $\tau_{cp,max} < \tau_f$ [30 and 90 MPa, respectively, in Fig. 6(a)], where $c_0 = 10$ MPa and $\tau_{GB} = 350$ MPa; and $\tau_{cp,max} > \tau_f$ [41 and 30 MPa, respectively, in Fig. 6(b)] where $c_0 = 20$ MPa and $\tau_{GB} = 400$ MPa. It can be seen that, in the first case, from the moment when the condition for slip transfer is

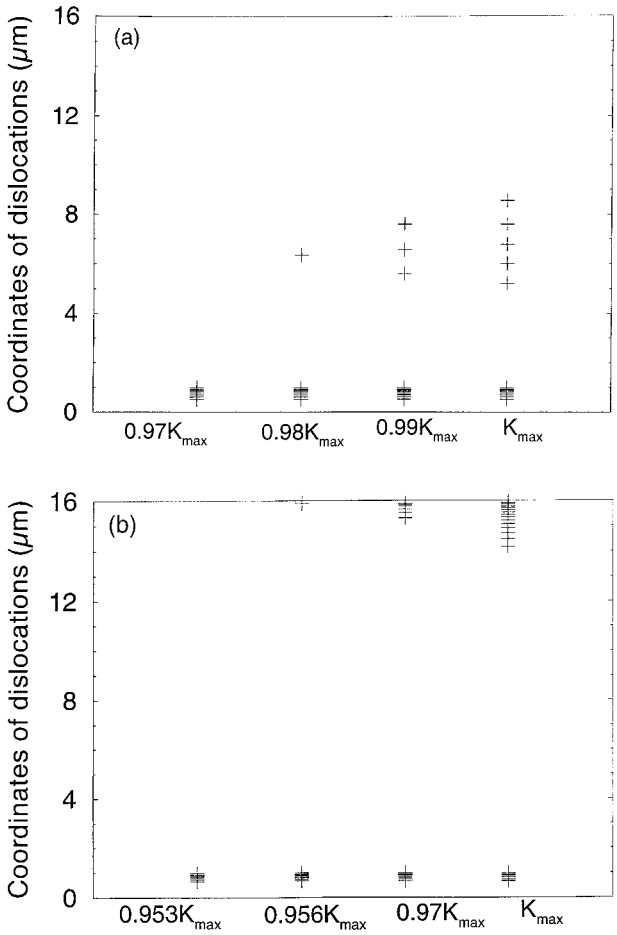

Fig. 6 Positions of the dislocations emitted by a crack tip located 1 μm away from a first grain boundary, and 16 μm from a second one, at various points of a load ramp in torsion. (a) $\tau_{cp,max}$ = 30 MPa, τ_f = 90 MPa, c_0 = 10 MPa and τ_{GB} = 350 MPa. (b) $\tau_{cp,max}$ = 41 MPa, τ_f = 30 MPa, c_0 = 20 MPa and τ_{GB} = 400 MPa (each plus represents a dislocation).

first met, plasticity extends progressively into the next grain (in this example it does not even reach the next grain boundary). In the second case, although dislocations that individually pass the first GB glide at once to the next one, slip transfer is more progressive than in the model of Navarro and De Los Rios[3] for which the blocked slip band, with all its dislocations, jumps to the next GB when a critical stress concentration is reached. It also appears that, due to the strong repulsive force of the pile up that pushes leading dislocations away, a second dislocation-free zone (in addition to that present between the crack tip and the trailing dislocation[1]) forms behind the grain boundary, as already mentioned by Pippan. This is in contrast with the predictions of dislocation distribution for a 'propagated slip band' of Tanaka *et al.*,[2] according to which the dislocation density is infinite on both sides of the GB.

Irregularity of Stage I kinetics

Simulations of Stage I growth at a constant stress range ($\Delta\tau/2$ = 36.5 MPa) have been performed, in reversed torsion, for a crack of initial half-length, a = 105 μm, in a polycrystal with a 15-μm mean grain size and a 30-MPa friction stress. The friction stress along the crack flanks was c_0 = 20 MPa. The calculated crack growth rates are plotted versus the crack length in Fig. 7, for various values of the critical stress for slip transfer at grain boundaries, τ_{GB}. These values of τ_{GB} are small enough to allow the crack to cross the grain boundaries, but slip transfer is achieved when the crack tip is very close to the GB ($\approx$ 0.1 μm), so that the corresponding points merge with those corresponding to the entry of the crack tip into the next grain. For τ_{GB} = 300 and 400 MPa, the size of the plastic zone, in microns, is indicated above (or below) each point of the curve. It can be seen that the condition for slip transfer beyond the first GB is met earlier and earlier in successive grains because of the increase in ΔK_{II}^{nom} associated with an increase in the number of dislocations emitted and piled up against the GB. But this does not produce a sudden acceleration, as slip transfer is progressive: the plastic zone may well extend over the GB, but a substantial fraction of the emitted dislocations may still be withheld by the GB and have a strong shielding effect. For example, for τ_{GB} = 400 MPa, the crack growth rate for a = 164 μm is smaller than for a = 160 μm, even though the plastic zone is larger, as in the former case, only

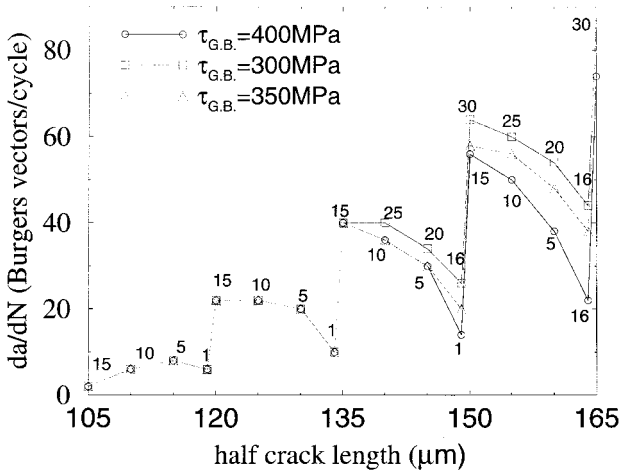

Fig. 7 Evolution of the growth rate for a Stage I crack (initial half-length 105 μm) propagating in a polycrystal with a 15-μm grain size, for various values of the critical stress for slip transfer at the grain boundaries, in reversed torsion ($\Delta t/2$ = 36.5 MPa, c_0 = 20 MPa, τ_f = 30 MPa).

three of the emitted dislocations have been transmitted to the second GB and eight of them remained stacked in a 1-μm-wide zone ahead of the crack tip. Unlike the case of unconstrained slip, there is therefore no correlation between the size of the plastic zone and the crack growth rate. It also appears that each time the crack tip enters a new grain there is a sudden acceleration. The magnitude of this acceleration depends on τ_{GB}. Figure 8 compares the distribution of emitted dislocations at K_{max} for crack half-lengths, a, of 149 and 150 μm, for various values of τ_{GB}. It is clear that the stronger the τ_{GB}, the higher the fraction of emitted dislocations withheld by the first GB for $a = 149$ μm (6/13 for $\tau_{GB} = 300$ MPa, 7/10 for 350 MPa and 7/7 for 400 MPa), and thus the larger the decrease in dislocation shielding when the crack passes the GB, this allows the emission of a larger number of dislocations.

Influence of the loading mode on GB crossing

It had been observed on a Co45Ni alloy, that for equivalent stress ranges it takes approximately twice as long for microcracks, once initiated, to cross the first GB encountered in reversed torsion than in push–pull,[11] but it was not clear whether this came merely from a slower transgranular growth rate, or if the interaction between microcracks and GBs was stronger in torsion. The present simulations throw some light on that point. Figure 9(a) compares the calculated stress concentrations due to the dislocations emitted by a microcrack and piled up against a very strong GB, at 1 μm from the GB in the next grain, and Fig. 9(b) compares the shear stress on the leading dislocation for a crack of initial half-length $a = 100$ μm propagating toward a GB, initially 50 μm away, for reversed torsion and push–pull loadings of equivalent stress ranges. First, it can be noticed that past a given crack length, the stress concentration in the next grain decreases because there are fewer dislocations emitted due to their increased shielding of the crack tip stress field. This is in contrast with the models of Tanaka *et al.*[2] and Navarro and De Los Rios,[3] according to which the stress concentration varies monotonically with the crack length until it reaches the GB. Anyway, the stress concentration in the next grain, as well as the shear stress on the leading dislocation, are both much higher in push–pull, because the opening stress increases K_{II}^{eff} and decreases K_{II}^{nucl}, so that many more dislocations are emitted and piled up than in torsion. Slip transfer on a coplanar slip plane is thus easier, which obviously facilitates GB crossing, not to mention the possibility to activate non-coplanar slip systems in the next grain that would be able to shield the mode I singularity, contrary

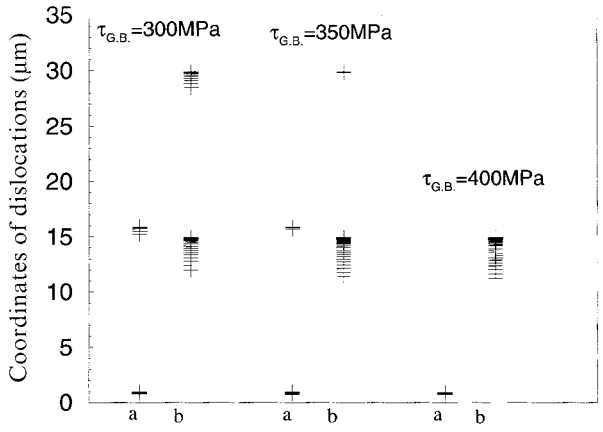

Fig. 8 Distribution of dislocations at K_{max}, at the tip of a Stage I crack, just before or after it crosses a grain boundary (distributions labelled a and b, respectively, corresponding to the points $a =$ 149 μm and 150 μm in Fig. 7) for various values of the critical stress for slip transfer at the grain boundaries in reversed torsion (each plus represents a dislocation).

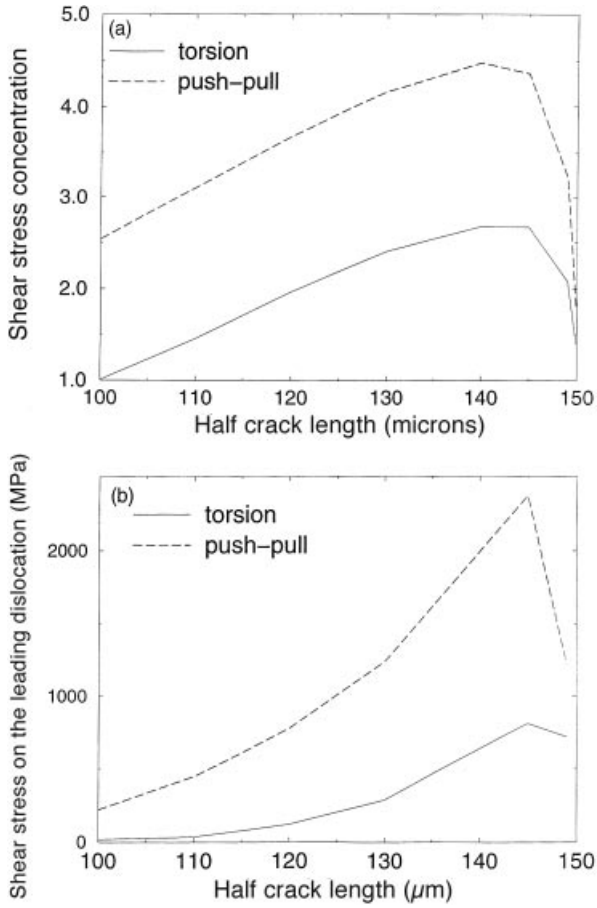

Fig. 9 Shear stress evaluations in reversed torsion and push–pull, for Tresca equivalent stress ranges. (a) Shear stress concentration in the next grain, at 1 μm from the boundary. (b) Shear stress on the leading dislocation at the tip of a Stage I crack (initial half-length 100 μm) propagating toward a grain boundary.

to coplanar slip. The explanation for the slower development of microcracks in torsion lies thus probably in the interaction with microstructural obstacles as well as in the slower transgranular growth rate predicted in Ref. 1 and illustrated in Fig. 3.

DISCUSSION

The interest of this approach compared to existing models based on continuously distributed dislocations is now discussed.

In previous work on Stage I cracks,[2,3] once the crack tip sliding displacement (CTSD) was deduced from the dislocation flux, growth laws of the type:

$$\frac{da}{dN} = B \cdot (\Delta \mathrm{CTSD})^m \quad \text{(Ref. 2)}$$

or

$$\frac{da}{dN} = B \cdot \Delta \mathrm{CTSD} \quad \text{(Ref. 3)}$$

were adopted, in which the constants B and m were unknown and could not be deduced from calculations performed on continuously distributed dislocations. These models do not, in fact, predict the crack growth rates. By contrast, the present approach is fully quantitative. However, it has to be recognized that the present model requires some data available only from sophisticated measurements (c_0, k_+, k_-, v_0, m, τ_f, τ_{GB}) or calculations (γ_{us}^u, γ_{us}^r, α) that make it unsuitable, for the time being, for engineering practice.

A second important difference is that the models mentioned above do not predict any threshold for Stage I crack growth when slip is not constrained. This is not consistent with experimental data on precracked single crystals, showing the existence of a finite, normal stress-dependent threshold stress intensity factor for crystallographic crack growth.[12] In the present approach, due to the consideration of a threshold stress intensity factor for dislocation emission at the crack tip, this experimental fact is predicted, whereas in the two other models, the dislocations necessary for the complete shielding of the crack singularity are considered as naturally available. This assumption does not seem appropriate for small stress ranges.

But the main difference between the present approach and pre-existing models is the attempt to capture the influence of the normal stress on crack tip plasticity and on the 'true' Stage I crack growth (as opposed to the 'extended' Stage I, involving secondary as well as coplanar slip, considered by Li[13]) which is believed to be essential for the analysis of multiaxial fatigue. Li derived an equation, of the same type as those from continuously distributed dislocation models quoted above, relating the growth rate to the vector CTD (total crack tip displacement, taking into account an opening component) evaluated by LEFM. This equation also contains an empirical proportionality constant that is not calculated. Moreover, this model is not yet able to deal with the influence of a compressive normal stress that does not induce any K_I term or any CTOD, but is well known to make Stage I crack growth slower, as the influence of such a stress on the mode II 'closure' term is not specified. The influence of grain boundaries is also ignored (although interesting work on this aspect has been performed by Li, using a finite element method).

The present simulations have to be considered as a tool for the understanding and analysis of Stage I cracking in multiaxial loading that should prove especially useful to analyse the influence of the loading path, when non-proportional loadings are considered, in future work.

CONCLUSIONS

The present approach, based on a simulation of discrete dislocation emission, glide and annihilation, at the tip of Stage I crack, assuming an influence of the normal stress on crack flank friction and dislocation emission was shown to reproduce important experimental facts.

(1) The existence of a normal stress-dependent threshold stress intensity factor, below which no propagation can occur, even in a single crystal, for lack of cyclic plasticity at the crack tip

(2) The variations in the crack growth rate or even the arrest of a crack due to interactions with microstructural obstacles which characterize Stage I crack growth.

A dual explanation for the slower development of Stage I cracks in reversed torsion compared to push–pull was also proposed, i.e. a slower transgranular propagation for unconstrained slip, mainly due to crack flanks friction, and a smaller stress concentration induced by constrained crack tip plasticity in the next grain.

REFERENCES

1 V. Doquet (1998) A first stage in the development of micromechanical simulations of the crystallographic propagation of fatigue cracks under multiaxial loading. *Fatigue Fract. Engng Mater. Struct.* **21,** 661–672.

2 K. Tanaka, Y. Akinawa, Y. Nakai and R. P. Wei (1986) Modelling of small fatigue crack growth interacting with grain boundary. *Engng Fracture Mech.* **24,** 803–819.

3 A. De Navarro and E. R. Los Rios (1988) Short and long fatigue crack growth: a unified model. *Phil. Mag. A* **57,** 15–36.

4 A. J. Wilkinson, S. G. Roberts and P. B. Hirsch (1998) Modelling the threshold conditions for propagation of Stage I fatigue cracks. *Acta Mater.* **46,** 379–390.

5 R. Pippan (1992) The condition for the cyclic plastic defor-

mation of the crack tip: the influence of dislocation obstacles. *Int. J. Fracture* **58,** 305–318.
6 C. A. Caracostas, H. M. Shodja and J. Weertman (1995) The double slip plane model for the study of short cracks. *Mech. Mater.* **20,** 195–208.
7 Y. Sun, G. E. Beltz and J. Rice (1993) Estimates from atomic models of tension-shear coupling in dislocation nucleation from a crack tip. *Mater. Sci. Engng A* **170,** 67–85.
8 K. M. Jassby and T. Vreeland, Jr (1970) An experimental study of the mobility of edge dislocations in pure copper single crystals. *Phil. Mag.* **21,** 1147–1168.
9 S. M. Ohr (1985) An electron microscope study of crack tip deformation and its impact on the dislocation theory of fracture. *Mater. Sci. Engng* **72,** 1–35.
10 W.-L. Li and J. C. M. Li (1989) The effect of grain size on fracture toughness. *Phil. Mag.* **59A,** 1245–1261.
11 V. Doquet (1997) Crack initiation mechanisms in torsional fatigue. *Fatigue Fract. Engng Mater. Struct.* **20,** 227–235.
12 Z. X. Tong, S. Lin and C. M. Hsiao (1986) The mechanism of fatigue crack propagation in pure aluminium single crystals. *Scripta Metall.* **20,** 977–982.
13 C. Li (1989) Vector CTD criterion applied to mixed mode fatigue crack growth. *Fatigue Fract. Engng Mater. Struct.* **12,** 59–65.